Journal of Sound and Vibration (1999) **220**(4), 729–748
Article No. jsvi.1998.1975, available online at http://www.idealibrary.com on IDEAL

DUAL DYNAMIC ABSORBER FOR THE TORSIONAL VIBRATIONS OF SYNCHRONOUS MOTOR-DRIVEN COMPRESSORS

B. O. Al-Bedoor and K. A. Moustafa

Mechanical Engineering Department, *King Fahd University of Petroleum & Minerals KFUPM Box* 841, *Dhahran* 31261, *Saudi Arabia*

AND

K. M. Al-Hussain

Dynamic Analysis Unit, *Saudi Aramco E*-7185, *Dhahran* 31311, *Saudi Arabia*

(*Received* 18 *July* 1997, *and in final form* 18 *September* 1998)

This paper presents a dynamic absorber to reduce the torsional vibrations exhibited during start-up of systems driven by synchronous motors. The dynamic absorber is comprised of two inertia rings connected, via spring-like material, to both the driver side (motor) and the driven side (compressor). The stiffness and inertia properties of the absorber are optimally tuned to match the torsional natural frequency of the system. A lumping technique is used to produce the dynamic model with non-linear flexible coupling. The results of the basic model are verified by using the results of previously published work on the modelling of non-linear flexible couplings. The numerical results on the dual dynamic absorber show excellent reduction in the vibration amplitudes as well as noticeable reduction in the vibration duration. Furthermore, the results of this study indicate that this kind of dynamic vibration absorber will contribute to solving, practically, the problem of torsional vibrations in systems driven by synchronous motors.

1. INTRODUCTION

The problem of vibrations encountered in torsional systems has become of great concern to designers and maintenance engineers as well as theoreticians. The concern has increased recently due to the need for using synchronous motors to drive large rotational systems. Synchronous motors are known to have mainly a two-part driving torque. One part is the average driving torque while the second part is the varying frequency oscillatory component. The oscillatory torque frequency varies from 0 to 120 Hz, which is twice the slipping frequency. In the start-up, generally, the frequency of the oscillating torque matches one or more of the torsional natural frequencies of the driven system. This leads to a high vibration amplitude that can cause failure of different system components and definitely reduces the fatigue life of system couplings. It has become evident that

0022–460X/99/090729 + 20 $30.00/0

a reliable and practically possible method for reducing these transient vibrations is highly demanded. This method is crucial to design, maintenance and to increasing the fatigue life of plants in service. It is noteworthy to mention that the meaning of transient vibrations in the literature, when synchronous motors are involved, should not be understood as caused by initial conditions. Actually, the porblem is of forcing type, but with a property of changing forcing frequency. Furthermore, a resonance condition is encountered when the frequency of excitation matches one of the system's natural frequencies. This resonance condition ceases when the forcing frequency moves away from the natural frequency of the system and this is the reason for the name transient vibrations.

Due to the nature of the problem, very few publications could be found. Most of the experimental and/or theoretical studies on this problem have been conducted by manufacturers who are usually conservative in releasing reports on their studies. According to Arnot [1], studies on transient torsional vibrations have been developing since the 1960s. In reference [1], a non-linear flexible coupling was introduced to reduce the transient vibrations in torsional systems. The study included both numerical and experimental results for a number of synthetic-rubber-compound hardness grades. Shadely *et al*. [2] reported a torsional vibration computational model for design purposes. They reported a transient-torsional vibration record for an actual coupling failed in torsion. In addition, they concluded their work by confirming the existence of a type of self-excited torsional vibrations in both numerical and laboratory results. Furthermore, Shadely *et al*. [2] observed unstable growth in torsional vibrations amplitudes when the mass moment of inertia of the load is more than twice the moment of inertia of the motor. In a paper on the transient analysis of synchronous motor trains by Szenasi and von Nimitz [3], the philosophy of optimum location of torsional critical speeds and resonance frequencies was discussed. It was concluded that for systems with massive motors, the presence of natural frequencies in the range of 0–120 Hz is usually unavoidable. At the same time, the authors of reference [3] recommended seeking proper designs of couplings to reduce the transient torsional vibrations and the resulting dynamic stresses to acceptable levels. Chen *et al*. [4] proposed a simplified reduced order model to study the transient behaviour in systems driven by synchronous motor. The intent was to work with a single differential equation only in the time interval were transients are expected. Chen [5] reported results of a study on the torsional vibrations of synchronous motor trains. A *P*-version of the finite element method was proposed; however, a conventional lumping technique example was demonstrated. It was concluded that non-linear analysis is required for systems with flexible couplings. Recently, Hamouda *et al*. [6] studied the effect of torsional vibrations on the salient pole synchronous motor-driven compressor. Their results showed that there is a need for taking care of torsional vibrations in the design stage. Among their results, Hamouda *et al*. [6], stated that sustained oscillations might continue even after the synchronous speed is reached if there is insufficient damping in the system. They recomended using shaft material that can withstand the expected high stresses.

One can conclude that torsional vibrations are very destructive and need to be considered in the design stage as well as after the system starts its operation. The

use of flexible couplings is one method that is practically available to reduce these torsional vibrations. Although flexible couplings, due to their inherent non-linearity, are able to provide good practical means of reducing transient vibrations, they are not without their drawbacks and problems. One important problem is that flexible rubber couplings put more restrictions on rotor balancing. Furthermore, flexible rubber couplings exhibit permanent deformations and hardening that lead to changes in their properties and affect their performance. The need for reducing the torsional vibrations in conjunction with the problems associated with flexible couplings highlighted the need for seeking other practical means for reducing these vibrations. A well known resort, when resonance conditions are encountered, is the dynamic absorber. The dynamic vibration absorber has received the attention of investigators over years [7–10]. Recently Lee and Moorhem [11] reported analytical and experimental analysis of a self-compensating balancer in rotating machinery. Despite the amount of research on dynamic vibration absorbers, little can be found on the application of the dynamic absorber to systems with rigid body and flexible modes. One problem that arises for these systems is where to attach this absorber. Furthermore, no application was found on using the dynamic absorber when the forcing frequency is time dependent.

The present work is devoted towards introducing a dynamic vibration absorber to reduce the torsional vibrations encountered in systems driven by synchronous motors. The work starts by developing the basic torsional system mathematical model and describing the characteristics of synchronous motors. The dual dynamic absorber is designed to be attached to both the motor and compressor sides and the equations of motion of the model including the dynamic absorber are derived. A numerical example that allows comparison of the results of the present work to those previously published is solved by using the Newmark-beta integration technique. Furthermore, results of numerical experiments that investigate the effect of the non-linear coupling are presented. Finally, the validity of the proposed dual dynamic absorber in reducing the torsional vibrations is investigated for both linear and non-linear couplings.

2. BASIC MODEL

2.1. THE SYNCHRONOUS MOTOR

Synchronous motors of the salient-pole type normally have a pulsating torque component with a frequency spectrum from 0 to 120 Hz during start-up conditions. The oscillatory component of the start-up torque develops as a result of slipping between the motor rotor and stator. The slipping frequency continues to decrease until full synchronization is reached. According to reference [12], the motor driving torque T_m at any instant can be expressed in the form

$$T_m = T_{avg} + T_{osc} \sin(\omega_{exc} t), \tag{1}$$

where T_{avg} is the average torque, T_{osc} is the amplitude of the oscillating torque, and ω_{exc} is the oscillating torque frequency (a list of nomenclature is given in the

Appendix). The oscillating torque frequency is twice the slipping frequency which is usually represented as

$$\omega_{exc} = 2\pi(2f_l)\left(\frac{N_{syn} - N_m}{N_{sys}}\right) \text{rad/s}, \tag{2}$$

where f_l is the line frequency which is normally 60 Hz, $N_{syn} = 120f_l/\#pole$ rpm and N_m is the motor rotor instantaneous speed.

For easier numerical programming, the motor torque can be expressed in terms of rotor angular displacement as

$$T_m = T_{ang} + T_{osc} \sin(\theta_{exc}), \tag{3}$$

where

$$\theta_{exc} = 2\pi(2f_l)\left(t - \frac{\theta_m}{N_{syn}2\pi/60}\right). \tag{4}$$

For each specific machine, the load–torque–speed relationships are normally supplied by the manufacturer.

2.2. LINEAR DYNAMIC MODEL

The conventional lumping technique in conjunction with Lagrange's equations is used to develop the model for the torsional vibrations of the system shown in Figure 1. In the lumping technique one considers that equivalent masses are concentrated at stations which are connected together by massless shafts. The shafts are considered to have stiffness effect as well accompanying damping effect. The model shown in Figure 1 which consists of a three-stage centrifugal compressor driven by a synchronous motor through a rubber coupling, spacer, and gear coupling, is considered. This model is similar to the one used by Chen [5]. The reduced order model obtained by considering the flexibility in the rubber coupling and the gear coupling in series is shown in Figure 2. By using Lagrange's

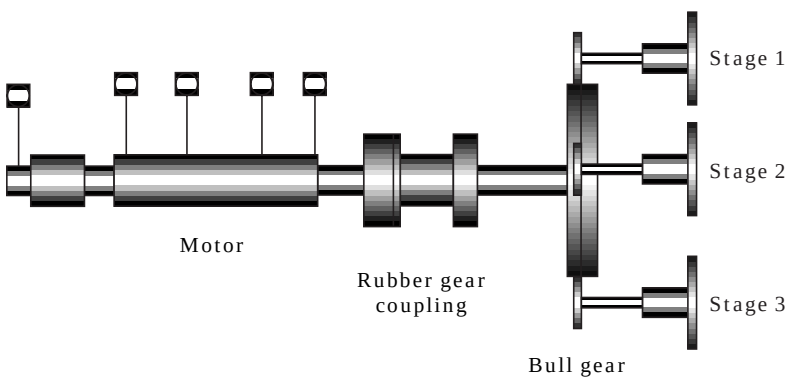

Figure 1. A multi-stage centrifugal compressor.

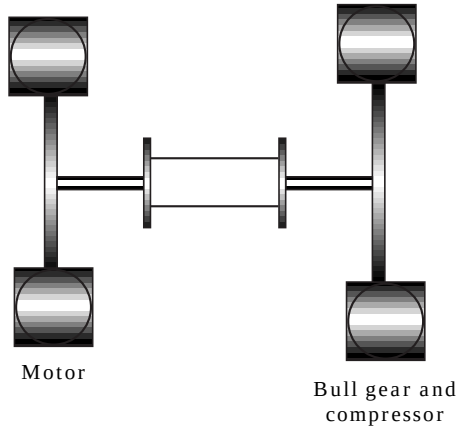

Figure 2. Reduced two degrees of freedom model.

equations, the equations of the two degrees of freedom model can be written in the form

$$\begin{bmatrix} J_1 & 0 \\ 0 & J_2 \end{bmatrix} \begin{Bmatrix} \ddot{\Phi}_1 \\ \ddot{\Phi}_2 \end{Bmatrix} + \begin{bmatrix} C_{eq} & -C_{eq} \\ -C_{eq} & C_{eq} \end{bmatrix} \begin{Bmatrix} \dot{\Phi}_1 \\ \dot{\Phi}_2 \end{Bmatrix} + \begin{bmatrix} K_{eq} & -K_{eq} \\ -K_{eq} & K_{eq} \end{bmatrix} \begin{Bmatrix} \Phi_1 \\ \Phi_2 \end{Bmatrix} = \begin{Bmatrix} T_m \\ -T_L \end{Bmatrix}, \quad (5)$$

where J_1 and J_2 are the motor inertia and the equivalent compressor inertia, respectively. The equivalent damping in the couplings is found with the fact that the gear and the rubber coupling are connected in series. This gives the equivalent damping as

$$C_{eq} = C_G C_R/(C_G + C_R), \quad (6)$$

where C_G and C_R are the damping coefficients for the gear coupling and the rubber coupling, respectively. Similar treatment of the stiffness results in an equivalent stiffness coefficient as

$$K_{eq} = K_G K_R/(K_G + K_R), \quad (7)$$

where K_G and K_R are the gear and rubber couplings stiffness coefficients, respectively.

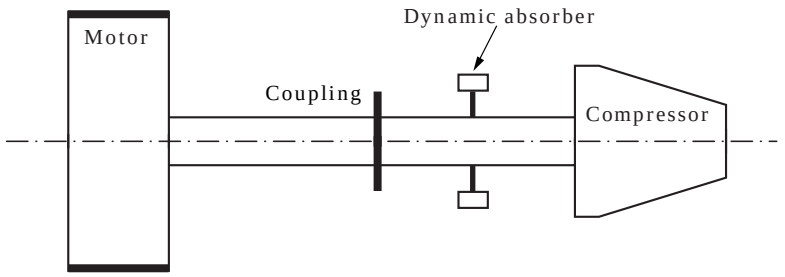

Figure 3. System with single dynamic absorber.

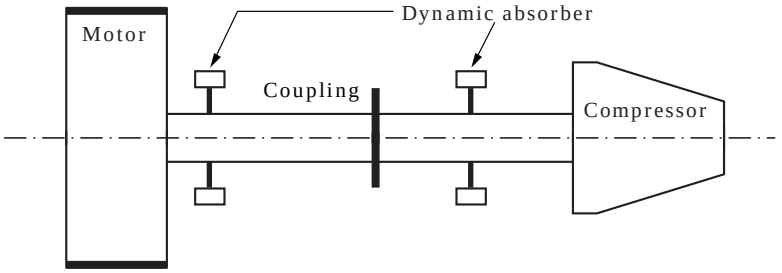

Figure 4. System with dual dynamic absorber.

One can now conclude that there are two types of coupling in the system; one is the gear coupling that is usually considered as linear due to its small deformation and it usually introduces a linear damping in the form of viscous damping. The second coupling is the flexible rubber coupling that exhibits large deformations and non-linear stress–strain relation.

2.3. NON-LINEAR COUPLING

The stiffness and damping properties of flexible rubber couplings are usually supplied by the manufacturer in the form of torque–angular deflections plots. Reference [1] contains experimental results on the stiffness and damping properties of the Holset rubber coupling. The linearized coupling stiffness and damping are given, respectively, in the form [1]

$$K_R = \partial(T_s)/\partial(\Delta\theta), \qquad C_R = K_R/M\omega_{exc}, \tag{8, 9}$$

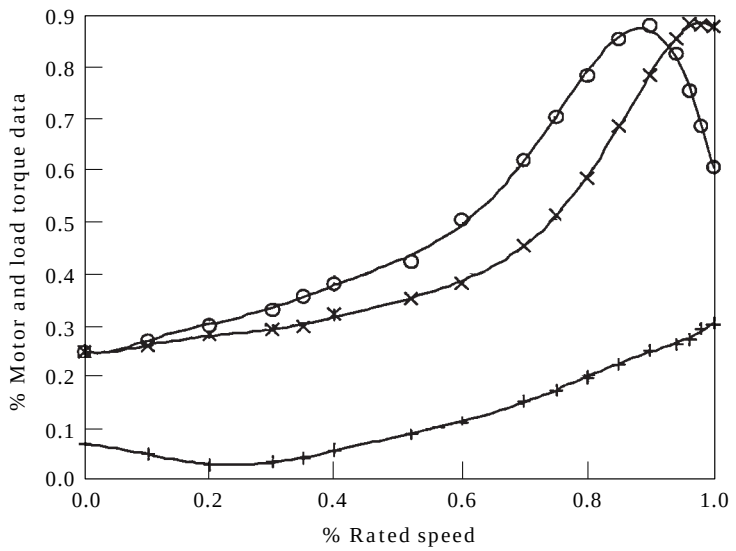

Figure 5. Torque–speed curve for the synchronous motor.

TABLE 1

Motor torque eighth order polynomial constants (% *rated torque*)

	A_0	A_1	A_2	A_3	A_4	A_5	A_6	A_7	A_8
T_{av}	191·4	−748·8	1162·0	−924·6	407·1	−98·8	12·4	−0·400	0·30
T_{os}	20·72	−145·38	323·81	−336·82	184·21	−53·19	7·54	−0·269	0·25
T_1	61·50	−224·23	318·75	−218·43	69·48	−6·17	−0·53	−0·139	0·07

where T_S is the instantaneous torque, M is the dynamic magnifier, which is a function of the coupling hardness grade, and ω_{exc} is the forcing frequency. Details on Holset flexible couplings can be found in references [1, 5].

3. DYNAMIC VIBRATION ABSORBER

Although the rubber type coupling has reduced the vibrations of the system treated in reference [5], to an extent, it has a disadvantage from the lateral dynamic point of view. The heavy overhung weight caused by this type of coupling makes it difficult for the manufacturer to design and to balance such a rotor. Therefore, it was decided in this study to explore other alternatives as an attempt to lower these torsional vibrations. One natural resort is a torsional absorber as a passive controller to this torsional vibration problem. In this study, the torsional absorber is an inertia ring which is to be connected to the system by using a spring-like material.

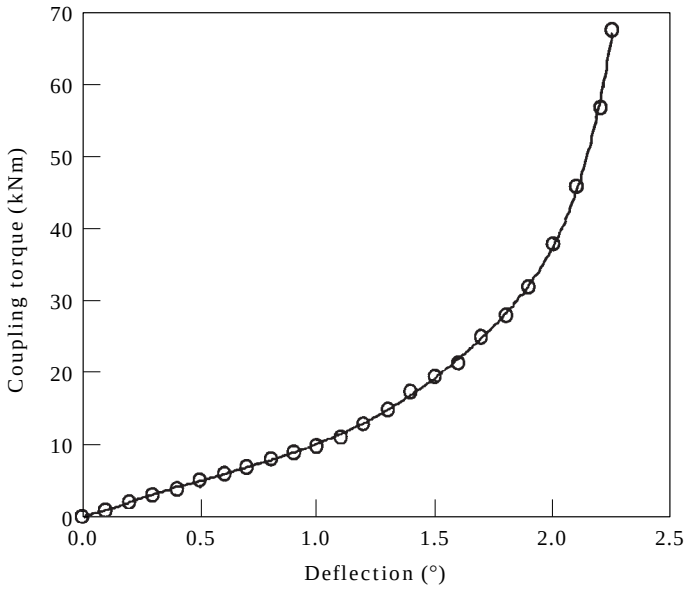

Figure 6. Rubber coupling torque versus angular deflection.

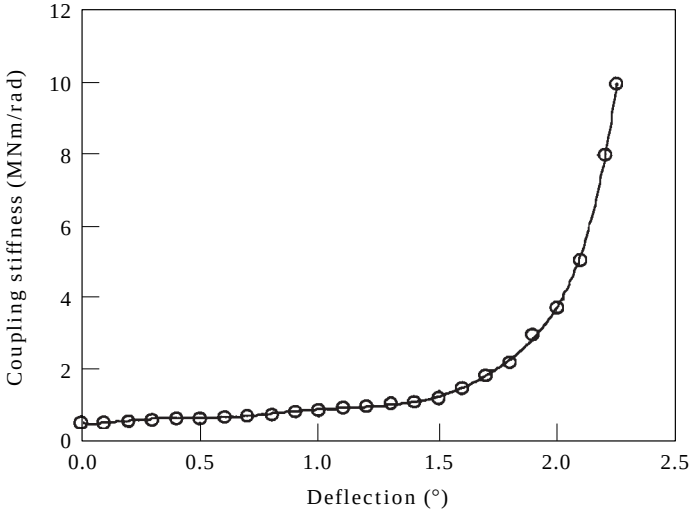

Figure 7. Rubber coupling torsional stiffness versus angular deflection.

3.1. SINGLE DYNAMIC ABSORBER

The single dynamic absorber arrangement is shown in Figure 3, where the dynamic absorber is attached to the compressor side of the system. By utilizing the system kinetic and potential energies in Lagrange's equations and considering the virtual work for the damping forces, the equations of motion of the system–absorber assembly can be represented in the matrix form

$$\begin{bmatrix} J_1 & 0 & 0 \\ 0 & J_2 + J_a & J_a \\ 0 & J_a & J_a \end{bmatrix} \begin{Bmatrix} \ddot{\Phi}_1 \\ \ddot{\Phi}_2 \\ \ddot{\Psi} \end{Bmatrix} + \begin{bmatrix} C_{eq} & -C_{eq} & 0 \\ -C_{eq} & C_{eq} & 0 \\ 0 & 0 & C_a \end{bmatrix} \begin{Bmatrix} \dot{\Phi}_1 \\ \dot{\Phi}_2 \\ \dot{\Psi} \end{Bmatrix} + \begin{bmatrix} K_{eq} & -K_{eq} & 0 \\ -K_{eq} & K_{eq} & 0 \\ 0 & 0 & K_a \end{bmatrix} \begin{Bmatrix} \Phi_1 \\ \Phi_2 \\ \Psi \end{Bmatrix} = \begin{Bmatrix} T_m \\ -T_L \\ 0 \end{Bmatrix}, \tag{10}$$

where Φ_1 is the rotational degree of freedom of the motor, Φ_2 is the compressor side degree of freedom and Ψ is the dynamic absorber rotational degree of freedom relative to the compressor rotational motion. The inertia, stiffness and damping properties of the absorber (i.e., J_a, K_a, C_a) are to be designed according to the original system natural frequencies. As a result, a modal analysis should be done as the system is semi-definite system with one rigid body mode. A procedure for dealing with such systems can be found in reference [13]. The kinetic energy of the original system can be written in the matrix form

$$T = \frac{1}{2} \begin{Bmatrix} \dot{\Phi}_1 \\ \dot{\Phi}_2 \end{Bmatrix}^{\mathrm{T}} \begin{bmatrix} J_1 & 0 \\ 0 & J_2 \end{bmatrix} \begin{Bmatrix} \dot{\Phi}_1 \\ \dot{\Phi}_2 \end{Bmatrix}. \tag{11}$$

Similarly the system potential energy is

$$U = \frac{1}{2}\begin{Bmatrix}\Phi_1\\ \Phi_2\end{Bmatrix}^{\mathrm{T}}\begin{bmatrix}K_{eq} & -K_{eq}\\ -K_{eq} & K_{eq}\end{bmatrix}\begin{Bmatrix}\Phi_1\\ \Phi_2\end{Bmatrix}. \tag{12}$$

The rigid body mode with zero natural frequency is one solution of the eigenvalue problem. Consequently, any other natural mode must be orthogonal to the rigid body mode. The constraint for this rigid body mode can be represented by the equation

$$\{\Phi^{(0)}\}[J]\{\Phi\} = 0. \tag{13}$$

For the rigid body mode let $\{\Phi^{(0)}\} = \{1\ \ 1\}^{\mathrm{T}}$; this will lead to the equation

$$J_1\Phi_1 + J_2\Phi_2 = 0 \tag{14}$$

from which $\Phi_2 = (-J_1/J_2)\Phi_1$. This condition can be represented by the operation

$$\begin{Bmatrix}\Phi_1\\ \Phi_2\end{Bmatrix} = \begin{bmatrix}1\\ -J_1/J_2\end{bmatrix}\{\Phi_1\}. \tag{15}$$

The transformation vector that eliminates the rigid body mode from the kinetic and potential energy expressions can be written as

$$\{A\} = \begin{bmatrix}1\\ -J_1/J_2\end{bmatrix}. \tag{16}$$

To this end, the reduced system kinetic and potential energy expressions can be compared to those for the complete system to yield the model inertia and modal stiffness, respectively, as

$$J_M = \{A\}^{\mathrm{T}}[J]\{A\}, \qquad K_M = \{A\}^{\mathrm{T}}[K]\{A\}. \tag{17, 18}$$

The resulting modal inertia and modal stiffness are the ones to be used in designing the optimum dynamic absorber parameters. For this purpose, one defines the frequency ratio

$$q = \omega_a/\omega, \tag{19}$$

where ω_a is the absorber's natural frequency and ω is the modal system natural frequency. Similarly one defines the inertia ratio μ as

$$\mu = J_a/J_M, \tag{20}$$

TABLE 2

Non-linear coupling torque and stiffness

	A_0	A_1	A_2	A_3	A_4	A_5	A_6	A_7	A_8
Torque (kN m)	6·07	−45·80	143·84	−244·99	246·57	−143·0	42·0	5·38	0·045
Stiffness (MN m/rad)	3·42	−27·69	91·056	−154·94	144·71	−72·37	17·42	−1·217	0·509

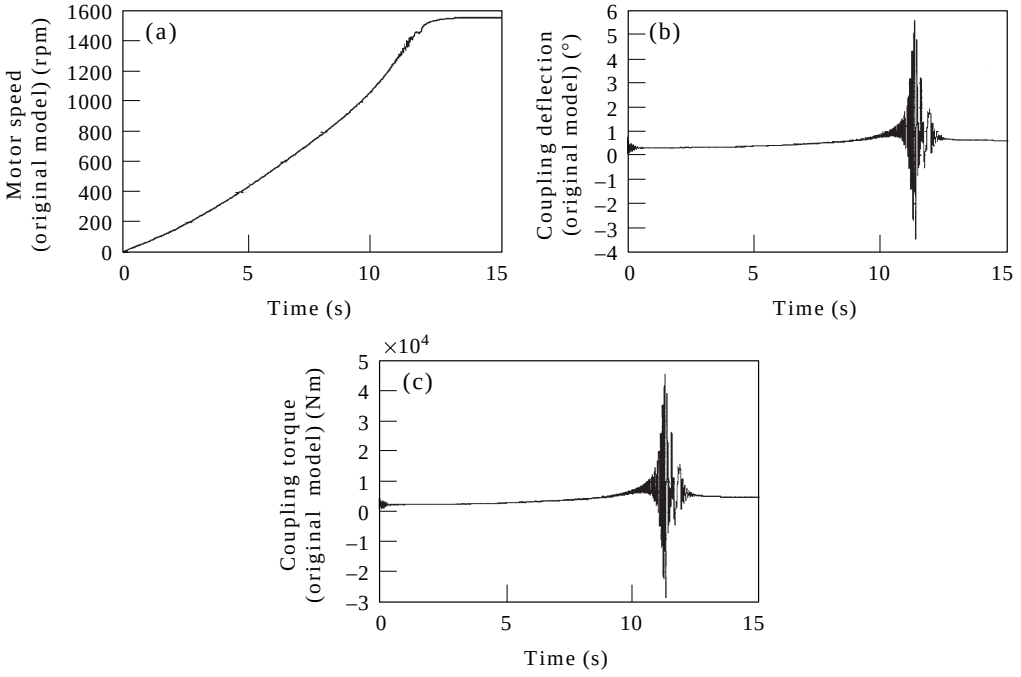

Figure 8. (a) Motor speed; (b) coupling deflection; (c) coupling torque. Linear rubber coupling with $K_R = 0{\cdot}47$ MN m/rad.

where J_a is the absorber mass moment of inertia and J_M is the system modal inertia. Following the optimization reported by Kelly [14], the parameters for the damped dynamic absorber can be found such that

$$q = \frac{1}{1+\mu}, \qquad K_a = (q\omega)^2 J_M \quad \text{and} \quad \zeta_{opt} = \sqrt{\frac{3\mu}{8(1+\mu)}}, \tag{21}$$

where, ζ is the optimum absorber damping ratio. The process of designing the dynamic absorber properties starts by assuming an appropriate inertia ratio μ; then the stiffness and damping parameters can be calculated from equation (21).

One important issue that arises when one thinks of the dynamic absorber for the system in hand is to which side the absorber should be attached, i.e., to the motor side or to the compressor side of the coupling. Absorbers are usually attached to locations with the highest possible motion of the system to extract maximum vibration energy. As shown in section 4, the system flexible mode shape shows maximum deflection at both ends, with the nodal point of zero deflection in between. This finding creates the idea of having two similar absorbers, at both sides of the system.

3.2. DUAL DYNAMIC ABSORBER

A schematic diagram of the system after installing the two similar dynamic absorbers is shown in Figure 4. By using Lagrange's equations,

the system–dual absorber equations of motion can be expressed in the matrix form

$$\begin{bmatrix} J_a & J_a & 0 & 0 \\ J_a & J_1 + J_a & 0 & 0 \\ 0 & 0 & J_2 + J_a & J_a \\ 0 & 0 & J_a & J_a \end{bmatrix} \begin{Bmatrix} \ddot{\Psi}_1 \\ \ddot{\Phi}_1 \\ \ddot{\Phi}_2 \\ \ddot{\Psi}_2 \end{Bmatrix} + \begin{bmatrix} C_a & 0 & 0 & 0 \\ 0 & C_{eq} & -C_{eq} & 0 \\ 0 & -C_{eq} & C_{eq} & 0 \\ 0 & 0 & 0 & C_a \end{bmatrix}$$

$$\times \begin{Bmatrix} \dot{\Psi}_1 \\ \dot{\Phi}_1 \\ \dot{\Phi}_2 \\ \dot{\Psi}_2 \end{Bmatrix} + \begin{bmatrix} K_a & 0 & 0 & 0 \\ 0 & K_{eq} & -K_{eq} & 0 \\ 0 & -K_{eq} & K_{eq} & 0 \\ 0 & 0 & 0 & K_a \end{bmatrix} \begin{Bmatrix} \Psi_1 \\ \Phi_1 \\ \Phi_2 \\ \Psi_2 \end{Bmatrix} = \begin{Bmatrix} 0 \\ T_m \\ T_L \\ 0 \end{Bmatrix}. \quad (22)$$

4. NUMERICAL RESULTS AND DISCUSSION

In order to gain insight into the behaviour of the torsional vibrations of systems driven by synchronous motors and to test the validity of the proposed method for reducing these vibrations, the data of Example 2 reported in reference [5] is simulated in the following sections.

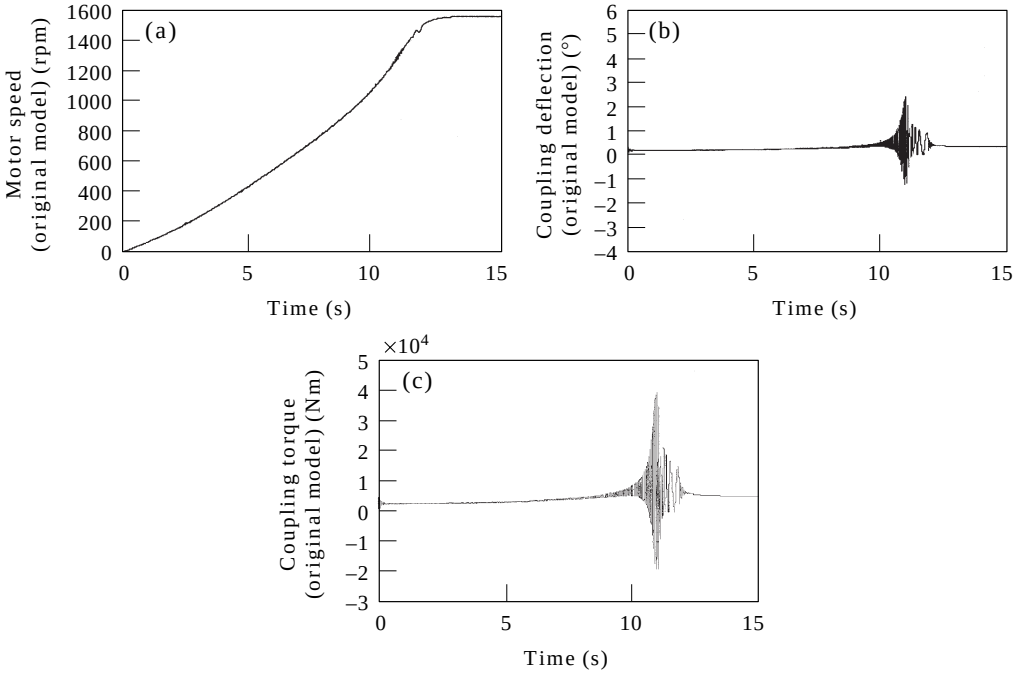

Figure 9. (a) Motor speed; (b) coupling deflection; (c) coupling torque. Linear rubber coupling with $K_R = 0{\cdot}987$ MN m/rad.

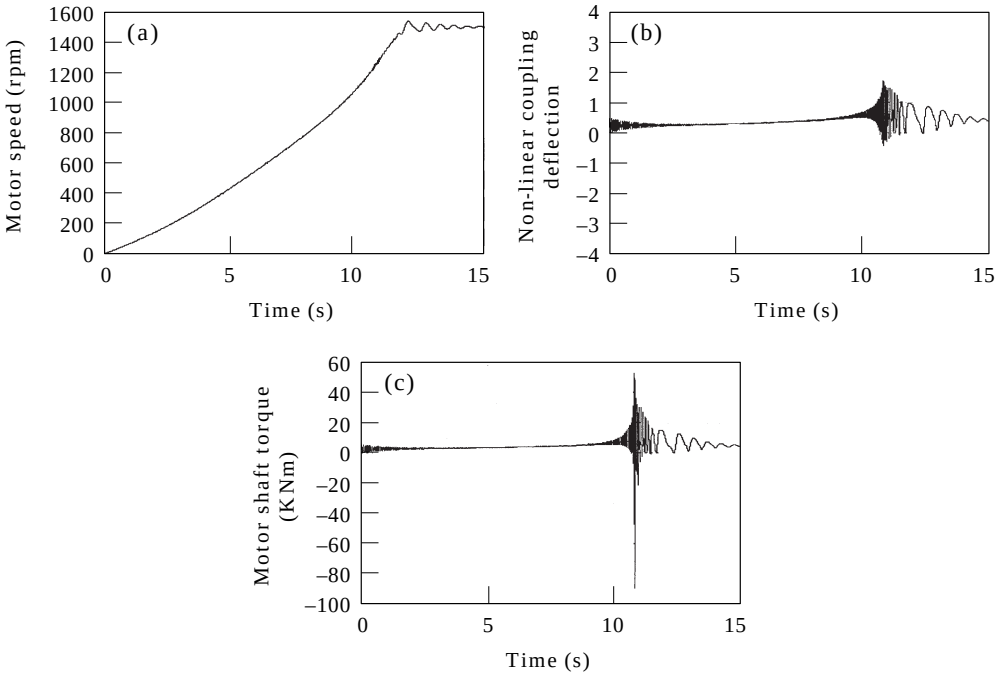

Figure 10. (a) Motor speed; (b) coupling deflection; (c) coupling torque. Non-linear rubber coupling.

4.1. MODEL DATA

A schematic diagram of the system is shown in Figure 1 with the reduced two degrees of freedom system shown in Figure 2. The motor is a four-pole 2237 kW rated at a speed of 1500 rpm. The motor rotor inertia $J_1 = 139$ kg-m^2 and the driven side compressor has an equivalent inertia $J_2 = 224$ kg-m^2 referred to the motor side. The motor–torque and the load–torque are shown in Figure 5. The

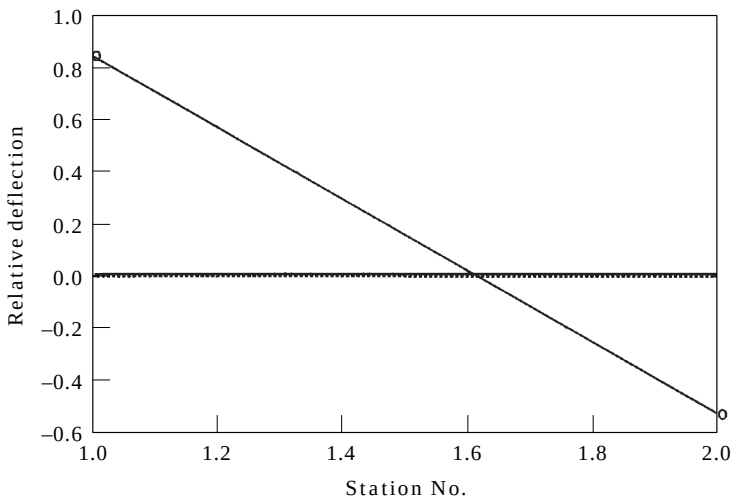

Figure 11. Original system flexible mode shape.

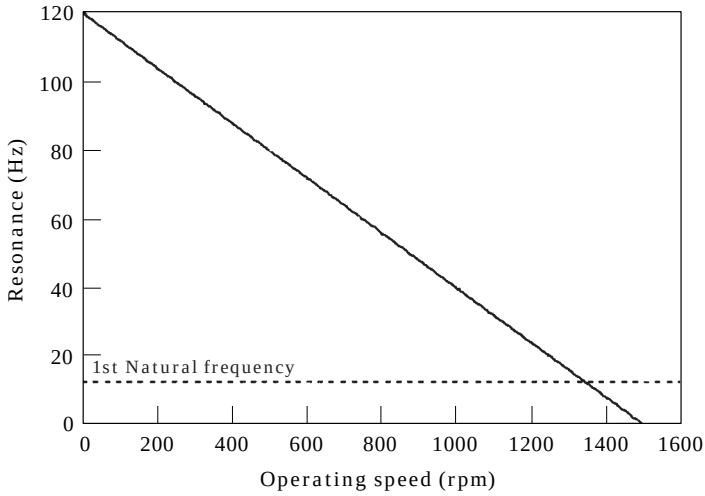

Figure 12. Original system interference diagram.

coefficients of the eighth order polynomial, that are obtained by curve fitting for the torque–speed relation of Figure 5, are shown in Table 1. The motor side and the compressor side are connected through gear and rubber couplings in series. The gear coupling has a linear stiffness $K_G = 9{\cdot}77 \times 10^7$ Nm/rad. On the other hand, the rubber coupling torque–deflection and stiffness–deflection curves, as taken from experimental data [5], are shown in Figures 6 and 7, respectively. Curve fitting is performed for the torque–deflection relation, Figure 6, and the coefficients are shown in Table 2.

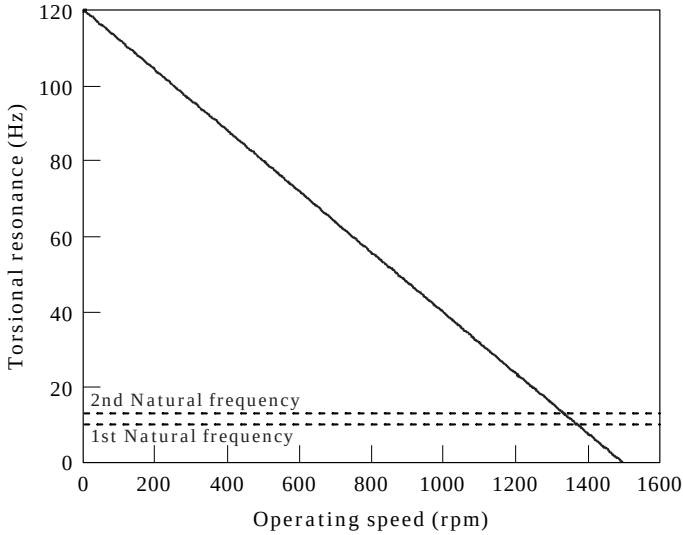

Figure 13. System interference diagram when a single absorber is attached to the compressor side.

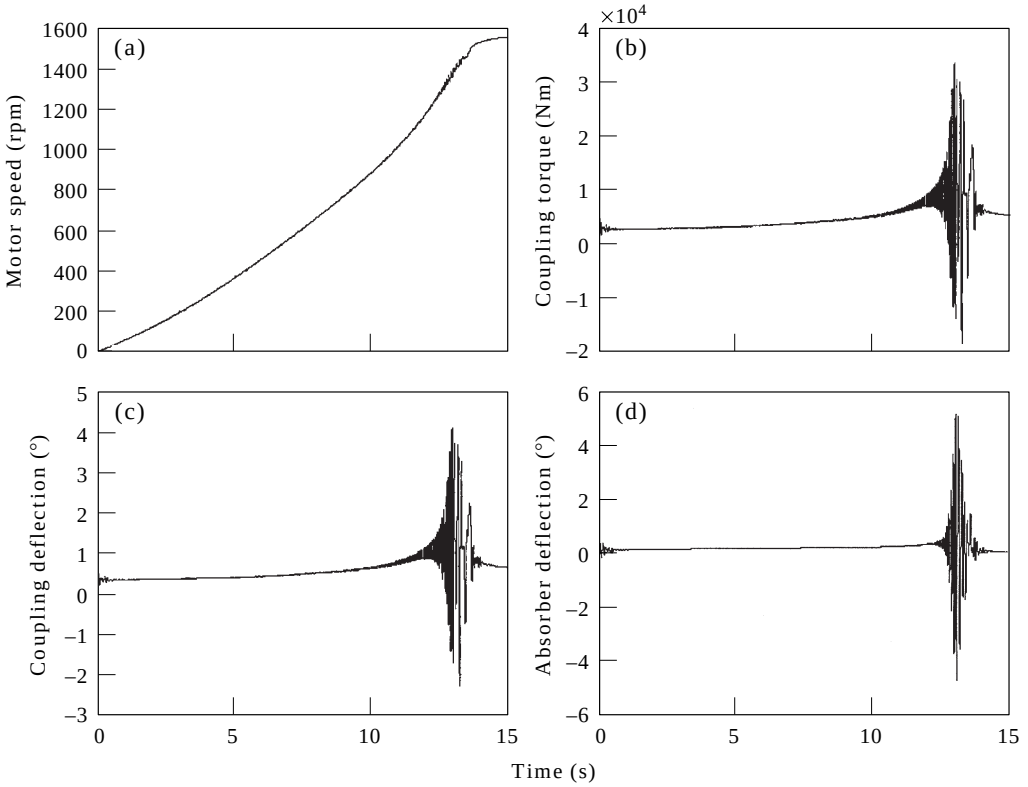

Figure 14. (a) Motor speed; (b) coupling torque; (c) coupling deflection; (d) absorber deflection. Linear rubber coupling with $K_R = 0{\cdot}987$ MN m/rad and a single dynamic absorber.

4.2. NEWMARK-BETA TECHNIQUE

The Newmark-beta method is known as an unconditionally stable numerical integration technique that can handle second order differential equations. The Newmark-beta algorithm [15] is programmed for this study where the time step is selected to be 1/10 of the highest frequency in the system. The constant parameters α and β are chosen as 0·5 and 0·25, respectively, to obtain an unconditionally stable scheme.

4.3. TRANSIENT RESPONSE: LINEAR AND NON-LINEAR

In order to validate the numerical technique used in this study, it is necessary to simulate cases reported in previous investigations [5]. For the linear rubber coupling with stiffness $K_R = 0{\cdot}47$ MN m/rad, the system responses are shown in Figure 8, in which part (a) shows the motor speed, part (b) shows the coupling deflection and part (c) shows the coupling dynamic torque. Figure 9 shows the same curves of Figure 8 but with a linear rubber coupling stiffness $K_R = 0{\cdot}987$ MN m/rad. It is clear that exactly the same results were obtained in reference [5]. The coupling deflection, as expected, is reduced when a higher coupling stiffness is used. This supported the need for using the actual non-linear analysis in reference [5]. The transient response obtained by using the actual

non-linear properties of the rubber coupling as supplied by the manufacturer are shown in Figure 10. It is shown that the maximum coupling deflection during transient vibration has reduced from 3·7° peak to peak in the linear case to 2° peak to peak in the non-linear simulation. Comparing the transient responses, from both linear and non-linear analysis, with the results of reference [5] shows excellent agreement and confirms the numerical technique adopted.

4.4. SINGLE DYNAMIC ABSORBER

The first step in designing the dynamic absorber is to find the characteristics of the original system. Eigenvalue analysis showed that the system has a torsional undamped natural frequency of 11·75 Hz. The corresponding mode shape is shown in Figure 11. This mode shape shows maximum deflection at both ends and one nodal point of zero deflection in between. The interference diagram, Figure 12, shows that the torsional excitation frequency matches the system natural frequency at around 80% of the motor running speed. Based on this information, the dynamic absorber is designed with the absorber inertia equal to 0·25 of the modal inertia which is 225 kg m^2. The optimum damping ratio for the absorber is chosen to be 0·278. After including the single dynamic absorber on the compressor side, the system natural frequencies are 10·97 and 12·84 Hz. The corresponding interference diagram is shown in Figure 13. The transient response

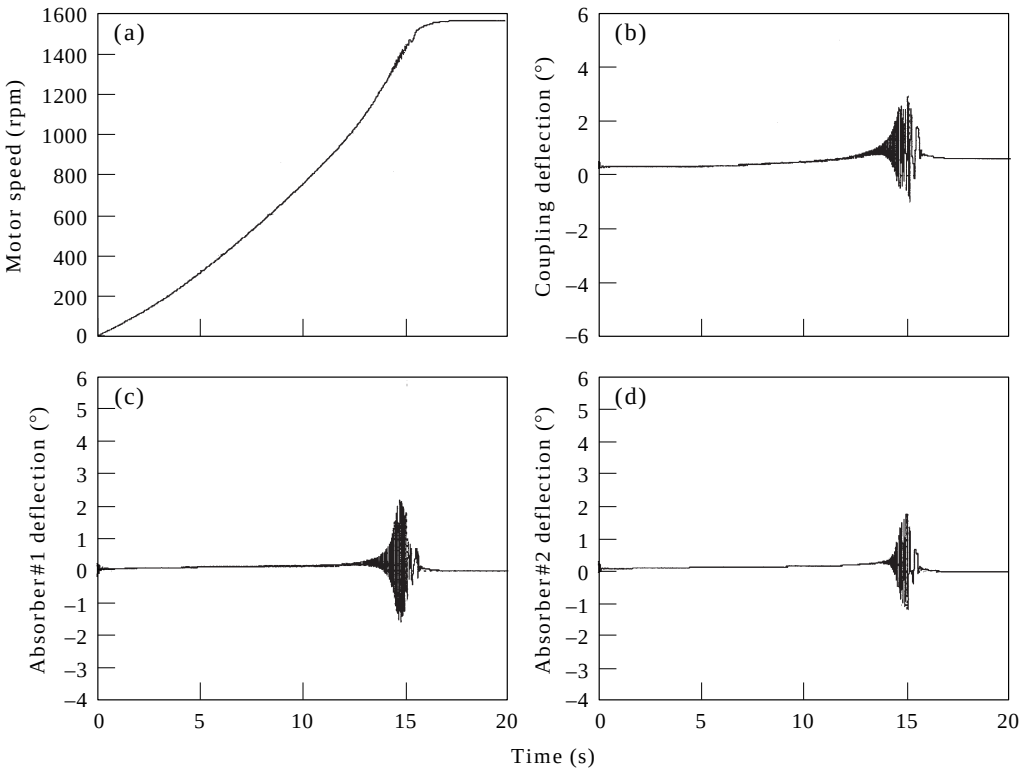

Figure 15. (a) Motor speed; (b) coupling torque; (c) coupling deflection; (d) absorber deflection. Linear rubber coupling with $K_R = 0{\cdot}987$ MN m/rad and dual dynamic absorber.

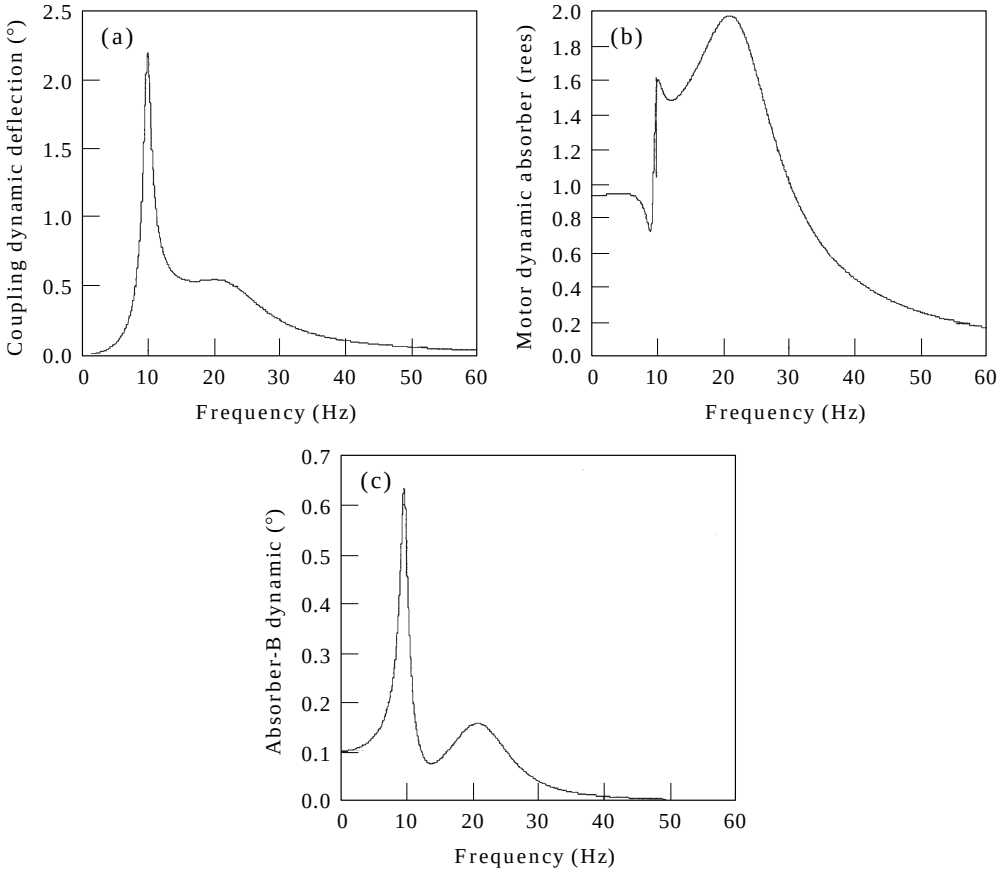

Figure 16. Frequency response of (a) the coupling deflection, (b) the motor side dynamic absorber and (c) the compressor side dynamic absorber.

analysis after fixing the absorber to the linear model with rubber coupling stiffness $K_R = 0{\cdot}987$ MN m/rad is performed and the results are shown in Figure 14. The motor speed is shown in Figure 14(a), Figure 14(b) shows the coupling torque, Figure 14(c) shows the coupling deflection and Figure 14(d) shows the absorber deflection. Comparison of the results of Figure 14 to the corresponding results of Figure 7 shows no significant reduction in the maximum peak to peak transient amplitudes, but the duration of the transient has reduced from about 4 s in Figure 7 to only around 2·5 s in Figure 14 when the absorber is installed. In Figure 14(b), the coupling torque is shown to be reduced, if compared to the torque of Figure 7, as a result of the dynamic absorber. The mode shape of the original system, Figure 11, and the fact that a single absorber attached to the compressor side has no significant effect, suggest attaching two similar absorbers at both sides of the system. The properties of both absorbers are the same and are calculated based on the modal properties of the system.

4.5. DUAL DYNAMIC ABSORBER

Adding one dynamic absorber at each side of the system was inspired by the system mode shape, Figure 11, and by taking note of the recommendation of reference [2] to exclude the situation where self-excited vibration that are expected to develop when the load inertia is more than twice the motor-rotor inertia. The motor side is exhibiting forced oscillations coming from the slipping effect and the compressor is oscillating as a result of the oscillatory torque transmitted through the system couplings. The same dynamic absorber that was designed in the previous section based on the modal inertia is added to each side of the system. The transient analysis is performed after the dual dynamic absorber is added to the linear system with $K_R = 0{\cdot}987$ MN m/rad and the results are shown in Figure 15. A significant reduction in the maximum peak to peak transient amplitude of the coupling deflection is shown in Figure 15(b). This reduction is almost the same as that obtained by using the non-linear rubber coupling analysis shown in Figure 10. Furthermore, a significant reduction in the vibration duration is shown, from that with the non-linear rubber coupling analysis. The dynamic absorbers' deflections are shown to be reasonable and can be tolerated; see Figures 15(c) and 15(d). To gain more insight into the system after installing the two dynamic absorbers, the frequency responses of the system are shown in Figures 16(a, b, c). The coupling deflection is shown in Figure 16(a) to have an

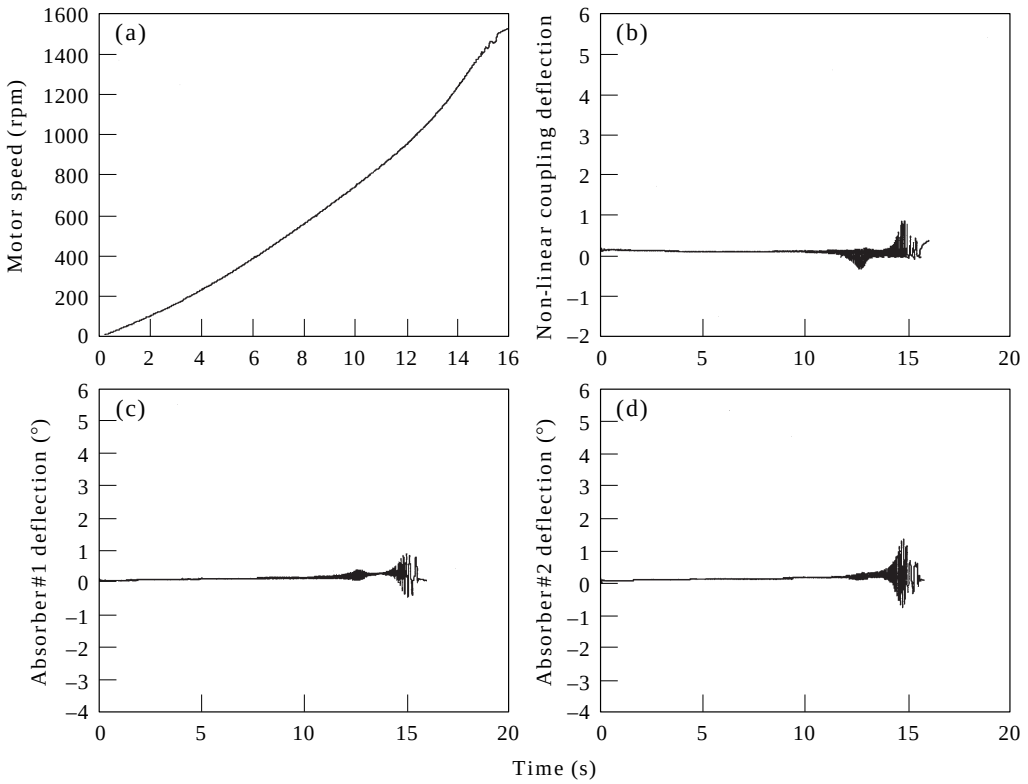

Figure 17. (a) Motor speed; (b) coupling torque; (c) coupling deflection; (d) absorber deflection. Non-linear rubber coupling with dual dynamic absorber.

amplitude of about 2·2° at a frequency of around 10 Hz which is the original system natural frequency and it is not affected by adding the absorbers. Figures 16(b) and 16(c) show the frequency responses of the motor and the compressor dynamic absorbers, respectively. One can recognize that using this dual dynamic absorber is giving better results than the non-linear coupling.

To study further the effect of using the dual dynamic absorber, simulation results on the system which is equipped with both the non-linear flexible rubber coupling and the dual dynamic absorber are shown in Figure 17. Excellent reduction in the coupling maximum peak to peak deflection is shown in Figure 17(b), if compared to Figure 10(b) and to the results of reference [5]. The peak to peak maximum amplitude in Figure 17(b) is about 1·2° while the maximum peak to peak amplitude of the non-linear coupling deflection in Figure 10(b) is 2·2°.

5. CONCLUSIONS

A dual dynamic absorber to reduce the torsional vibrations exhibited during start-up of systems driven by synchronous motors has been described. The dual dynamic absorber is two inertia rings connected, via spring-like material, to both the driver side (motor) and the driven side (compressor). The stiffness and inertia properties of the dual absorber are optimally tuned to match the torsional natural frequencies of the system. A lumping technique is used to produce the dynamic model with non-linear flexible coupling. The results of the basic model are verified by using the results of previously published work on the modelling of non-linear flexible couplings. The numerical results on the dual-dynamic-absorber show excellent reduction in the transient vibration amplitudes as well as noticeable reduction in the torsional vibration duration.

ACKNOWLEDGMENT

The support of King Fahd University of Petroleum & Minerals is greatly appreciated.

REFERENCES

1. R. M. Arnott 1993 *Holset Company Research Report*, *VDI Berichte NR* 1082. Nichtlinear Charakteristik Torsionelastticher Kuppungen bie Groben Schwingungsamplitudeen.
2. J. R. Shadely, B. L. Wilson and M. S. Dorney 1992 *Transactions of the ASME*, *Journal of Vibration and Acoustics* **114**, 226–231. Unstable self-excitation of torsional vibration in AC induction motor driven rotational systems.
3. F. R. Szenasi and W. W. von Nimitz 1978 *Proceedings of the Seventh Turbomachinery Symposium*, 111–117. Transient analysis of synchronous motor trains.
4. H. M. Chen, W. D. Mclaughlin and B. S. Malanoski 1983 *Proceedings of the Twelfth Turbomachinery Symposium*, 115–119. A generalized and simplified transient torque analysis for synchronous motor drive trains.
5. W. Chen 1995 *Transactions of the ASME*, *Journal of Vibration and Acoustics* January, 152–162. Torsional vibration of synchronous motor driving train using *P*-method.

6. R. M. HAMOUDA, M. A. BADAR and A. I. ALOLAH 1996 *IEEE Transactions on Energy Conversion* **11**(3), 531–538. Effect of torsional dynamics on a salient pole synchronous motor-driven compressors.
7. J. P. DEN HARTOG 1956 *Mechanical Vibrations*. New York: McGraw–Hill; fourth edition.
8. R. G. JACQUOT and J. E. FOSTER 1977 *Transactions of the ASME*, *Journal of Engineering for Industry* February, 138–141. Optimal cantilever dynamic vibration absorbers.
9. H. N. OZGUVEN and B. CANDIR 1986 *Journal of Sound and Vibration* **111**(3), 377–390. Suppressing the first and second resonances of beams by dynamic vibration absorbers.
10. G. L. GLAUSSER, J. N. JUANG and J. L. SULLA 1993 *Proceedings of the Field Institute Communications* **2**, 197–214. Optimal active vibration absorber: design and experimental results.
11. J. LEE and W. K. V. MOORHEM 1996 *Transactions of the ASME*, *Journal of Dynamic Systems*, *Measurements*, *and Control* **118**, 468–475. Analytical and experimental analysis of a self-compensating dynamic balancer in a rotating mechanism.
12. J. M. VANCE 1988 *Rotordynamics of Turbo Machinery*. New York: Wiley.
13. L. MEIROVITCH 1967 *Analytical Methods in Vibrations*. New York: Macmillan.
14. G. S. KELLY 1993 *Fundamentals of Mechanical Vibrations*. New York: McGraw–Hill.
15. K. J. BATHE 1982 *Finite Element Procedures in Engineering Analysis*. Englewood Cliffs, NJ: Prentice–Hall.

APPENDIX: NOMENCLATURE

$\{A\}$ transformation vector
$[C]$ damping matrix
C_a dynamic absorber damping coefficient
$\overline{C}_{eq}$ equivalent damping coefficient
C_G gear damping coefficient
C_R rubber coupling damping coefficient
f_l line frequency (60 Hz)
G gear coupling
$[J]$ inertia matrix
J_1 motor inertia
J_2 compressor inertia
J_a dynamic absorber inertia
J_M modal inertia
K_a dynamic absorber stiffness
K_{eq} equivalent torsional stiffness
K_G gear coupling stiffness
K_M modal stiffness
K_R rubber coupling stiffness
N_m motor speed
N_{syn} synchronous speed
T kinetic energy
T_m motor torque
T_{avg} average motor torque
T_{osc} coefficient of the oscillating torque component
T_L load torque
T_s instantaneous torque
t time
q frequency ratio
α Newmark-beta integration constant

β Newmark-beta integration constant
Φ_1 motor angular motion
Φ_2 compressor angular motion
ω_{exc} excitation frequency (rad/s)
Ψ_1 motor dynamic absorber motion relative to the motor
Ψ_2 compressor dynamic absorber motion relative to the compressor
μ inertia ratio
ξ damping ratio
ξ_{opt} optimum damping ratio